

A Damage Mechanics-Based Fatigue Life Prediction Model for Solder Joints

Hong Tang

NEC Electronics Corporation,
Detroit, MI

Cemal Basaran

Mem. ASME
Associate Professor and Director,
UB Electronic Packaging Laboratory,
University at Buffalo, SUNY,
Buffalo, NY 14260
e-mail: cjb@eng.buffalo.edu

A thermomechanical fatigue life prediction model based on the theory of damage mechanics is presented. The damage evolution, corresponding to the material degradation under cyclic thermomechanical loading, is quantified in a thermodynamic framework. The damage, as an internal state variable, is coupled with unified viscoplastic constitutive model to characterize the response of solder alloys. The damage-coupled viscoplastic model with kinematic and isotropic hardening is implemented in ABAQUS finite element package to simulate the cyclic softening behavior of solder joints. Several computational simulations of uniaxial monotonic tensile and cyclic shear tests are conducted to validate the model with experimental results. The behavior of an actual ball grid array (BGA) package under thermal fatigue loading is also simulated and compared with experimental results.

[DOI: 10.1115/1.1536171]

1 Introduction

With the increasing use of surface mount bonding technology in microelectronics industry, the reliability concerns for solder joints are increasing exponentially. Eutectic solder alloys are most commonly used bonding materials in electronic packaging, which provide electrical and thermal interconnection, as well as mechanical support. The temperature fluctuations due to device internal heat dissipation and ambient temperature changes, along with the coefficient of thermal expansion (CTE) mismatch between the soldered layers, result in thermo-mechanical fatigue of the solder joints. Progressive damage in solder balls eventually leads to device failure. Fatigue life prediction of solder joints is critical to the reliability assessment of electronic packaging.

Standard state of practice in the electronic industry for the number of cycles to failure prediction is based on using empirical relations, such as Coffin-Manson approach. Typically, using the CTE differential between the bonded components, the maximum elastic and plastic strain in the solder joint is calculated. Most of the time, using the plastic strain value, Coffin-Manson curves are used to predict the fatigue life of solder joints. Usually this approach yields very conservative results for BGA packages, Zhao et al. [1]. Recently, numerous physics-of failure based models have been developed for the evaluation of reliability of solder alloys under thermo-mechanical fatigue loading, such as Busso et al. [2], Dasgupta et al. [3], Frear et al. [4], McDowell et al. [5], Basaran et al. [6,7], Chow and Yang [8], Basaran and Chandaroy [9], Qian et al. [10]. The majority of these models use plastic strain as the criterion of fatigue life prediction. But plastic strain alone cannot appropriately reflect the physical mechanism of fatigue damage. Because, plastic strain is not a unique value in numerical analysis. In other words one could obtain different plastic strain value for the same state of stress by following different path to get to the final point in the stress space, Desai and Sirdardane [11]. In addition, these models are mostly developed for monotonic loading and use isotropic hardening, hence, cannot be directly used for cyclic loading.

The damage evolution function used in this study is based on the second law of thermodynamics and uses entropy as a damage metric. Earlier, Basaran and Yan [12] have shown that the entropy, which is a measure of disorder in a system, can be used as a damage metric in solid mechanics. The damage evolution is in-

corporated into a unified viscoplastic constitutive model to characterize the cyclic fatigue behavior of solder joints under thermo-mechanical loading. The constitutive model is implemented into ABAQUS through its user defined material subroutine.

In order to validate the model and ABAQUS implementation testing was performed. An actual BGA package was subjected to thermal cycling in an SuperAGREE thermal chamber and plastic strain field was measured by means of Moiré interferometry. Using ABAQUS, with the implemented constitutive model, same thermal cyclic tests were simulated and results were compared.

The behavior of solder joints is simulated as a nonlinear quasi-static initial boundary value problem. The nonlinear problem is solved incrementally by dividing the time interval into numbers of successive time steps. For each time step, global equilibrium equations, under specific loading and boundary conditions and defined material properties, are solved by ABAQUS with implicit time integration scheme to obtain the strain increment.

At each strain increment, along with the initial condition determined by last time step, the stress and internal state variables are integrated and updated within a user defined material subroutine for each Gauss point. An implicit trapezoidal time integration scheme is used for viscoplastic strain computations. ABAQUS can check the residual forces of the global equilibrium equations and iteratively reach the convergence at each step.

2 Constitutive Model

Experimental results indicate that the contribution of the elastic strain component to low cycle fatigue life is negligible compared to the contributions of creep strain. The time-dependent creep strain dominates the low-cycle fatigue life of solder joints, Zhao et al. [1]. This is due to the fact that eutectic and near-eutectic solder alloys are regularly expected to perform at high homologous temperature ($0.5-0.8 T_m$) due to their low melting point (183°C). At high homologous temperatures, materials experience significant creep deformation. A thermo-viscoplastic constitutive model is, therefore, essential for modeling solder behavior.

In order to model primary, secondary and tertiary creep stages of near eutectic solder, a creep rate function is needed. Steady-state plastic deformation kinetics of most metals and alloys at high homologous temperatures can be described by Dorn creep equation, Stone and Rashid [13]. Kashyap and Murty [14] have experimentally shown that grain size can significantly affect creep behavior of Pb/Sn solder alloys. Based on their lab test data results they proposed the following creep law, which is a modified ver-

Contributed by the Electronic and Photonic Packaging Division for publication in the JOURNAL OF ELECTRONIC PACKAGING. Manuscript received by the EPPD Division, December 10, 2001. Associate Editor: Y.-H. Pao.

sion of Dorn equation. In this study the equation was further modified by adding the last term to account for multiple directional effect.

$$\dot{\varepsilon}_{ij}^{vp} = \frac{A \Delta E b}{k T} \left(\frac{\langle F \rangle}{E} \right)^n \left(\frac{b}{d} \right)^p \exp \left(- \frac{Q}{RT} \right) \frac{\partial F}{\partial \sigma_{ij}} \quad (1)$$

where F is the yield function, which will be discussed further later; $\langle \cdot \rangle$: Macauley brackets, $\langle F \rangle = F$ if $F \geq 0$; $\langle F \rangle = 0$ if $F < 0$; A : a dimensionless material constant; $\Delta = \Delta_0 \exp(-Q/RT)$ is a diffusion coefficient; Δ_0 is the temperature-independent frequency factor. For alloys, Δ_0 can be calculated by $\Delta_{0Pb/Sn} = N_{Pb} \Delta_{Sn} + N_{Sn} \Delta_{Pb}$, Smithells [15]. Where N_{Pb} and N_{Sn} are the fractional concentrations of Pb/Sn and Δ_{Sn} and Δ_{Pb} are the intrinsic chemical diffusion coefficients. Δ_{Sn} is $0.8 \text{ cm}^2/\text{s}$, and Δ_{Pb} is $0.28 \text{ cm}^2/\text{s}$, Friedel [16]. In this study, $\Delta_{0Pb/Sn}$ is taken equal to $0.488 \text{ cm}^2/\text{s}$; Q : creep activation energy for plastic flow. Based on the Arrhenius plot, activation energy is obtained as: $Q = 44.7 \text{ KJ/mol}$ for temperatures lower than 408 K , and $Q = 81.1 \text{ KJ/mol}$ for temperatures higher than 408 K Kashyap and Murty [14]; R : universal gas constant = $8.314 \text{ J/K.mol} = 8.314 \text{ N.m/K.mol}$; T : absolute temperature in Kelvin; E : Young's modulus; b : characteristic length of crystal dislocation. In this study, b is taken equal to the Burgers vector of pure Sn (3.18 \AA), Friedel [16]; k : Boltzmann's constant = $1.38 \times 10^{-23} \text{ J/K} = 1.38 \times 10^{-20} \text{ N.mm/K}$; d : average grain size; p : grain size exponent. Kashyap and Murty [14] obtained $p = 3.34$ based on creep test data on Pb40/Sn60 solder alloy at different temperatures and different grain sizes; n : is stress exponent for plastic deformation rate. Kashyap and Murty [14] showed that stress exponent n is not significantly influenced by the test temperature or grain size, it is obtained as 1.67 from creep tests.

The stress-strain relation can be given as follows after some derivations:

$$\{d\sigma_{ij}\}_n = \left([C_{ijkl}^e]^{-1} + \Delta t_n \chi \left[\frac{\partial \tilde{\varepsilon}_{kl}^{vp}}{\partial \sigma_{ij}} \right]_n \right)^{-1} \left(\{d\varepsilon_{kl}^{\text{total}}\}_n \right) - \Delta t_n \left\{ \tilde{\varepsilon}_{kl}^{vp} \right\}_n + \left(\chi \left[\frac{\partial \tilde{\varepsilon}_{kl}^{vp}}{\partial T} \right]_n \{dT_n\} \{I_{kl}\} \right) - (\alpha_T dT_n \{I_{kl}\}) \quad (2)$$

where $\{d\sigma_{ij}\}_n$ is the total stress increment vector; $[C_{ijkl}^e]^{-1}$ is the elastic constitutive matrix; $\Delta t_n = t_{n+1} - t_n$ is time step; $\chi = 0.5$ is employed corresponding to implicit trapezoidal rule, which is a unconditionally stable algorithm; $\tilde{\varepsilon}_{kl}^{vp}$ is viscoplastic strain rate; dT is the temperature increment; α_T is coefficient of thermal expansion; $\{I_{kl}\}$ is a diagonal identity matrix.

A von Mises type yield surface, F , with isotropic and kinematic hardening and coupled with internal state variable of damage, is used in the constitutive model.

$$F = \bar{\sigma}_{\text{eff}} - R - (1 - D)\sigma_y \quad (3)$$

where $\bar{\sigma}_{\text{eff}} = \sqrt{3/2}(\mathbf{s} - \mathbf{X}') : (\mathbf{s} - \mathbf{X}')$; $\bar{\sigma}_{\text{eff}}$ is the von Mises stress; \mathbf{s} is the deviatoric stress tensor; \mathbf{X}' is the deviator of back stress \mathbf{X} ; R is the evolution of the size of yield surface; σ_y is the initial size of the yield surface; D is the internal state variable of damage.

The kinematic hardening rule is adapted from Armstrong et al., [17] and Chaboche [18], and coupled with damage. \dot{X}_{ij} is the increment of back stress tensor

$$\dot{X}_{ij} = a \left[\frac{2}{3} X_{\infty} \varepsilon_{ij}^{vp} (\dot{I} - D) - X_{ij} \dot{p} (I - D) \right] \quad (4)$$

where $\dot{p} = \sqrt{2/3} \dot{\varepsilon}^{in} : \dot{\varepsilon}^{in}$; $\dot{\varepsilon}^{vp}$ is the increment of inelastic strain tensor; \dot{p} is the increment of the inelastic strain trajectory; X_{∞} , a are material constants, obtained from monotonic tensile test data.

For isotropic hardening, an exponential function is used [18], and coupled with damage

$$\dot{R} = c(R_{\infty} - R)\dot{p}(I - D) \quad (5)$$

where R_{∞} is a material constant of the asymptotic value of the size of elastic domain; c is a material constant.

In order to simulate cyclic fatigue behavior of materials, there is a need for a progressive degradation model. Damage mechanics provides us a basic framework to develop damage evolution models. Considering the effect of internal damage variable, the stress-strain relation can be defined as, Kachanov [19]

$$d\sigma_{ij} = (I - D) C_{ijkl} d\varepsilon_{kl} \quad (6)$$

where $d\sigma_{ij}$ is the increment of stress tensor; C_{ijkl} is the effective thermal elasto-viscoplastic constitutive matrix; $d\varepsilon_{kl}$ is the increment of the effective strain tensor; D is the damage variable of the current state.

Damage process corresponding to degradation of microstructure is, in general, irreversible. The numerical models of damage evolution proposed in the literature usually use a damage surface, similar to yield surface, and use the irreversible plastic strain as the primary metric (Kachanov [19], Rabotnov [20], Valanis [21], Chaboche and Lesne [22], Murakami [23], Krajcinovic [24], Ju [25], Lemaitre [26], Bazant [27], Chow and Chen [28], Voyiadjis and Thiagarajan [29]). Under mutiaxial loading conditions, the maximum plastic strain and damage can localize at different locations in the material [3]. Solomon and Tolksdorf [30] have shown that using dissipated energy alone does not lead to a unique damage value. Loading and strain rate significantly vary the energy dissipated in the system. Based on the second law of thermodynamics, Basaran and Yan [12] have shown that the entropy can be used as a unique damage metric. Based on Basaran and Yan's theory, the damage evolution function can be obtained as follows:

$$D = 1 - e^{-\Delta e - \Delta \phi / N_0 k T / \bar{m}_0} \quad (7)$$

where

$$\Delta e - \Delta \phi = \frac{1}{\rho} \left(\int_{\varepsilon_0}^{\varepsilon} \sigma_{ij} d\varepsilon_{ij}^{vp} \right) - \int_{t_0}^t \frac{1}{\rho} \frac{\partial q_i}{\partial x_i} dt + \int_{t_0}^t \dot{\gamma} dt \quad (8)$$

where $\Delta e, \Delta \phi$ are increments of internal energy and free energy, respectively; σ_{ij} , $d\varepsilon_{ij}^{vp}$ are total stress and increment of inelastic strain respectively; q_i is the heat flux tensor; $\dot{\gamma}$ is the distributed internal heat production rate per unit mass; dt is the increment of time; N_0 is the Avogadro's constant; k is the Boltzman's constant; \bar{m}_0 is the average molecule quantity/mol; T denotes absolute temperature; ρ is specific mass.

Comparison of the damage evolution model discussed here with other models in the literature and physics behind it is discussed in great detail in [12].

3 Finite Element Simulations of Laboratory Tests

In order to verify the validity of the model and ABAQUS implementation, the finite element simulation results are compared with the laboratory test data from Adams [31], Skipor et al. [32]; McDowell et al. [5] and from our own testing.

Adams [31] performed a series of tensile test on Pb40/Sn60 bulk solder specimens at different strain rates and different temperatures. Figure 1 shows the comparison between Adams' test data and the finite element simulations at the strain rate $1.67\text{E-}2$.

Skipor et al. [32] performed several uniaxial tensile tests on Pb37/Sn63 dog-bone-shaped solder specimens at different strain rates and different temperatures. Figure 2 shows the comparison between Skipor's test data and the finite element simulation for the strain rate of $1.0\text{E-}1$.

McDowell et al. [5] performed several uniaxial tensile tests on Pb36/Sn62/Ag2 solder specimens at different strain rates and different temperatures. Figure 3 shows the comparison between McDowell's test data and the finite element simulations for strain rate of $1.0\text{E-}2$.

ABAQUS

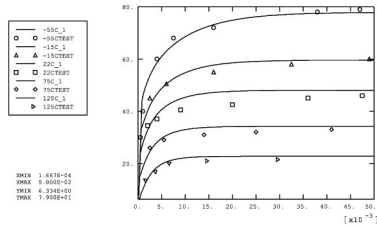


Fig. 1 Uniaxial extension simulation (solid lines) versus Adams's test under strain rate 1.67E-2 and different temperature

ABAQUS

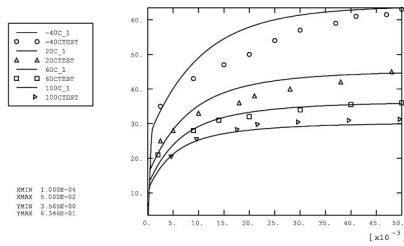


Fig. 2 Uniaxial extension simulation (solid lines) versus Skiper's test under strain rate 1.0E-1 and different temperature

ABAQUS

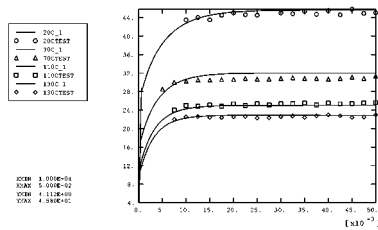
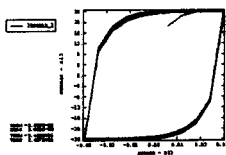
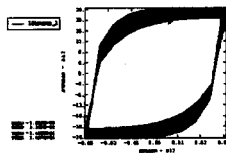


Fig. 3 Uniaxial extension simulation (solid lines) versus McDowell's test under strain rate 1.0E-2 and different temperature

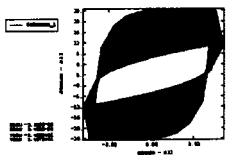
ABAQUS



ABAQUS



ABAQUS



ABAQUS

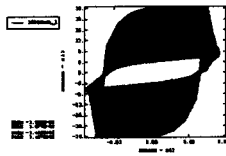
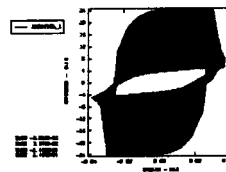


Fig. 4 Strain-stress hysteresis loop curves for 20, 100, 400, 700 cycles (inelastic strain range=0.04, 35°C)

ABAQUS



ABAQUS

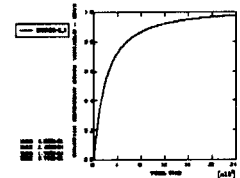
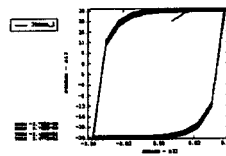


Fig. 5 Strain-stress hysteresis loop curves for 1010 cycles and damage evolution time-history (inelastic strain range = 0.04, 35°C)

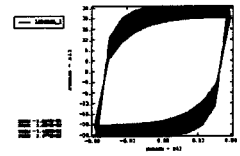
Comparisons reflect good correlations between test data and computational simulations. Due to page limitations not all comparison data are shown.

The most important advantage of damage mechanics based fatigue life prediction model is that it can simulate the cyclic softening behavior of material, which is corresponding to the material deterioration under cyclic loading. Several numerical simulations of simple cyclic shear tests are made by the damage mechanics based model, and compared with the fatigue test results of Pb40/Sn60 solder alloys by Solomon [33]. Solomon [33] performed cyclic simple shear tests on Pb40/Sn60 solder joints under isothermal displacement controlled conditions, with different plastic strain ranges. Solomon [33] published the number of cycles to failure for each plastic strain range he tested. The author defined the failure as 90% load drop in ultimate stress. Figures 4–9 show the simulations of strain-stress hysteresis loops under different cycles and different inelastic strain ranges and certain temperatures. It is easily observed that the hysteresis energy dissipation in the system reduced as the material degradation increases with the number of fatigue cycles increases. Figures 5, 7, and 9 in addition

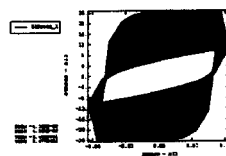
ABAQUS



ABAQUS



ABAQUS



ABAQUS

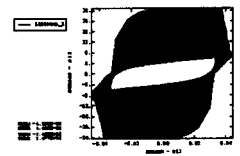
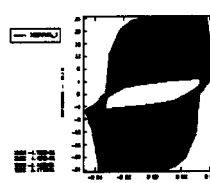


Fig. 6 Strain-stress hysteresis loop curves for 20, 100, 600, 1100 cycles (inelastic strain range=0.03, 35°C)

ABAQUS



ABAQUS

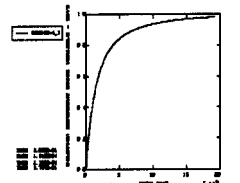


Fig. 7 Strain-stress hysteresis loop curves for 1010 cycles and damage evolution time-history (inelastic strain range = 0.03, 35°C)

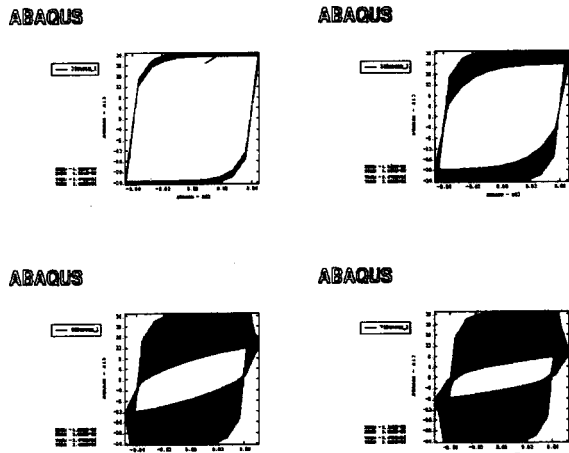


Fig. 8 Strain-stress hysteresis loop curves for 20,100,600,1500 cycles, (inelastic strain range=0.025, 35°C)

to cyclic stress-strain curves also show the damage accumulation as a function of time. In Fig. 10, the number of cycles to failure versus inelastic strain range is presented. Figure 10 shows the comparison between Solomon's test data and the ABAQUS finite element simulations.

Computer simulation is also performed for the fatigue behavior of Pb37/Sn63 solder joints in an actual BGA electronic package under cyclic thermal loading. The cross section of the BGA package tested is shown in Fig. 11. FR-4 printed circuit board (PCB) and polymer connector layer are connected by Pb37/Sn63 solder joints. Only half of the packaging is plotted and meshed for simu-

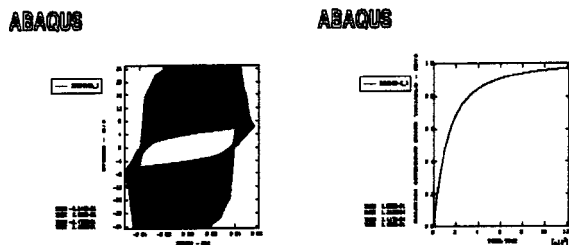


Fig. 9 Strain-stress hysteresis loop curves for 2000 cycles and damage evolution time-history (inelastic strain range =0.025, 35°C)

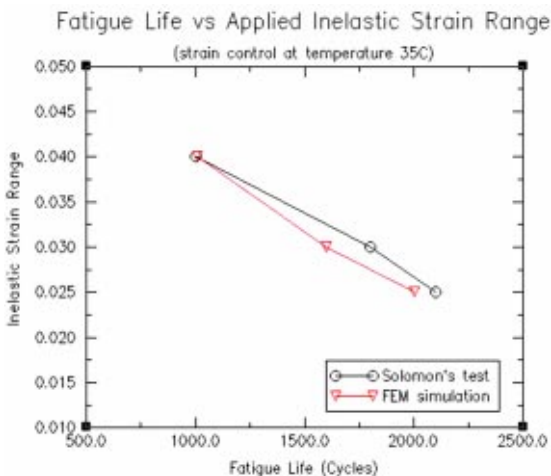


Fig. 10 Comparison of fatigue life (Solomon's test versus FEM)

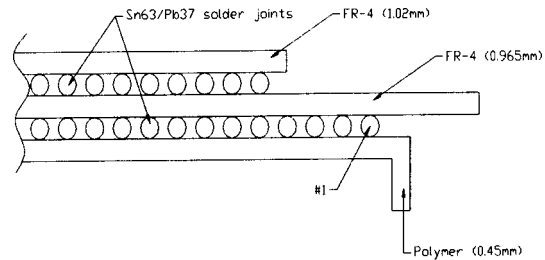


Fig. 11 Cross section of BGA electronic package

lation due to the structural symmetry. In ABAQUS 2-D plane-strain eight-node elements were used. Each solder joint is discretized by 16 elements. Basaran and Zhao [34] have shown that rate-dependent models do not suffer from mesh dependence due to softening; hence, a relatively course mesh yields very accurate results.

The package shown above was subjected to the thermal loading profile shown in Fig. 12. A Super AGREE thermal chamber was used for thermal cycling. Specimens were periodically taken out to measure inelastic strain accumulation in each solder joints using Moiré interferometry system. Details of this testing are given in [1,35]. During testing and FEA simulation the package is fixed at the both ends of the middle FR-4 PCB layer. In finite element simulations, FR-4 PCB and polymer layer are considered as linear elastic and solder joints as nonlinear elasto-viscoplasticity with damage evolution. Material parameters used for finite element simulations are given in Table 1.

Thermally induced shear strain in solder joints, due to the CTE mismatch between FR-4 PCB and polymer layer, are cyclic in nature, and they result in thermo-mechanical fatigue of solder joints. Experiment results show that shear strain dominates

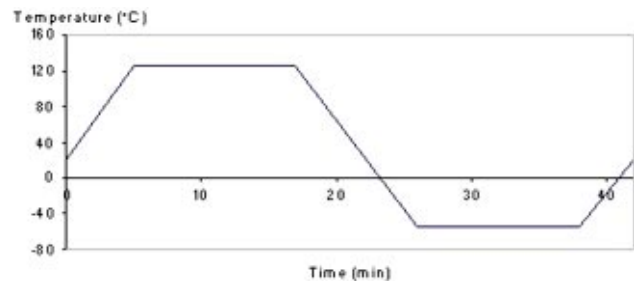


Fig. 12 The thermal loading profile of one cycle

Table 1 Material parameters of BGA electronic packaging (T: temperature in Kelvin)

| | FR-4 | Polymer | Solder |
|---|--------------------|---------|--------------|
| Young's modulus (Gpa) | 17.4 | 11.0 | |
| Poisson's ratio | 0.35 | 0.25 | |
| CTE (ppm/°C) | 16.0 | 48.0 | 24.7 |
| Parameters of solder alloy: | | | |
| Young's modulus (GPa): $E = 62.0 - 0.067 T$ | | | |
| Shear modulus (GPa): $G = 24.3 - 0.029 T$ | | | |
| Poisson's ratio: $\mu = E/(2G) - 1.0$ | | | |
| Kinematic hardening parameters | | | |
| $X_{\infty} = 35.26 - 0.069 T$ (MPa) | | | |
| $\alpha = 159.0 + 0.89 (T - 273.15)$ | | | |
| Isotopic harding parameters | | | |
| σ_y (MPa) | R_{∞} (MPa) | | ^c |
| $62.07 - 0.15 T$ | 6.0 | | 600.0 |
| Viscoplastic flow parameters | | | |
| A | Q (J/mole) | d (mm) | p |
| 5.8E9 | 44.7E3 | 3.5E-3 | 3.34 |
| | | | n |
| | | | 1.67 |

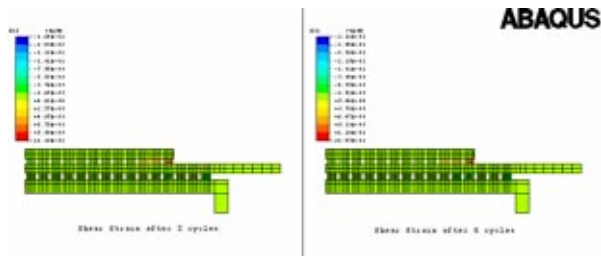


Fig. 13 Shear strain after two and four thermal cycles (with damage model implemented into ABAQUS)

thermal-fatigue in solder joints. Normal and peeling strain are smaller than shear strain by an order of magnitude [1]. Yet, when the damage accumulation is calculated all strain components are taken into account. Numerical simulations of shear strain are shown in Figs. 13–15. Figure 16 shows averaged inelastic shear strain accumulation in solder joint no. 1 versus the number of thermal cycles for FEA and Moiré interferometry measurement results. The finite element results of shear strain of the solder joint are in good correlation with the Moiré interferometry test data. During testing highest strain was always observed in solder joint no. 1. Therefore, the results of inelastic strain are plotted for that joint. It should be pointed out that inelastic strain accumulation is not linear from cycle to cycle. On the other hand, in Coffin-Manson approach, a single plastic strain value is used to define fatigue life. Therefore in practice the fatigue life of BGA packages obtained from lab tests is usually longer than the fatigue life computed by Coffin-Manson based models.

The simulations of damage distribution among solder joints are shown in Figs. 17–19. The damage distribution provides important information for design of optimization and reliability. Figure 20 shows the simulation of damage evolution of the critical solder joint. In Fig. 20 damage value does not reach the value of one which means total failure, because we did not perform thermal cycling and Moiré interferometry measurements up to failure. The damage evolution is an integrated reflection of material degradation under fatigue loading, rather than just determined by plastic strain or strain energy density, which were used as fatigue life

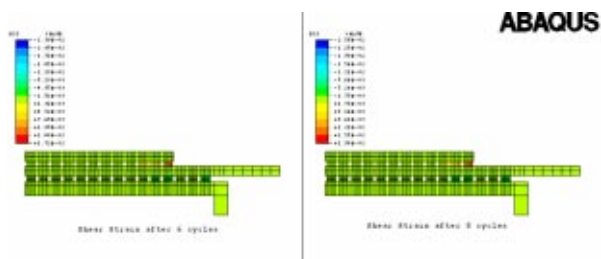


Fig. 14 Shear strain after six and eight thermal cycles (with damage model implemented into ABAQUS)

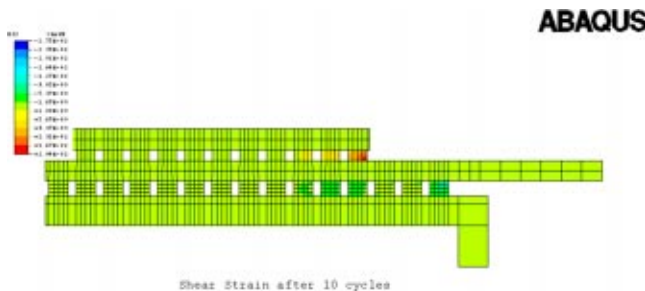


Fig. 15 Shear strain after 10 thermal cycles (with damage model implemented into ABAQUS)

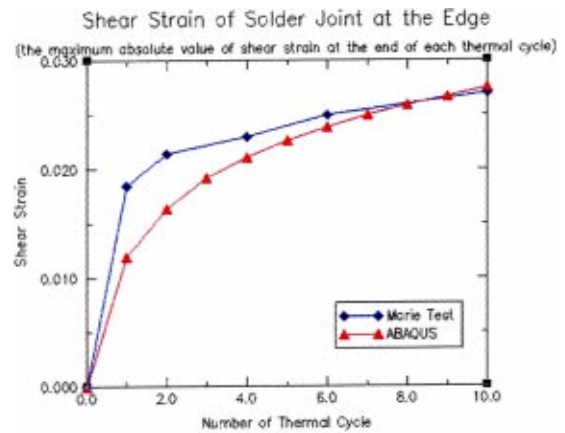


Fig. 16 Comparison of finite element simulation results with Moiré interferometry test data

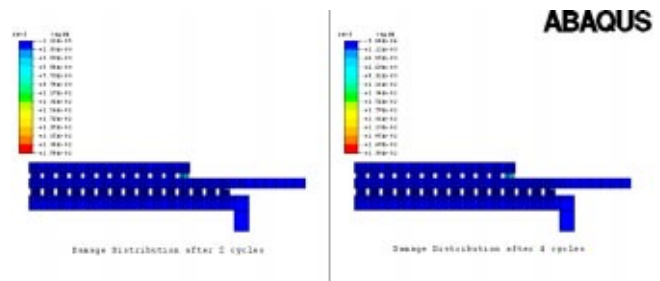


Fig. 17 Damage distribution after two and four thermal cycles (with damage model implemented into ABAQUS)

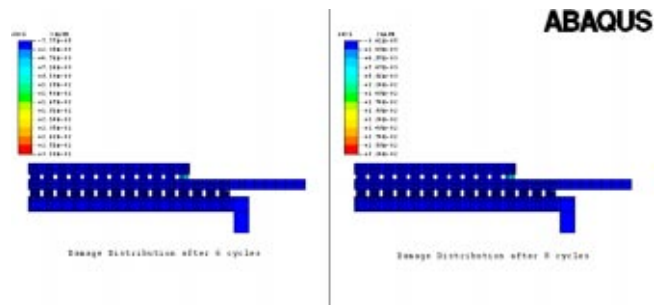


Fig. 18 Damage distribution after six and eight thermal cycles (with damage model implemented into ABAQUS)

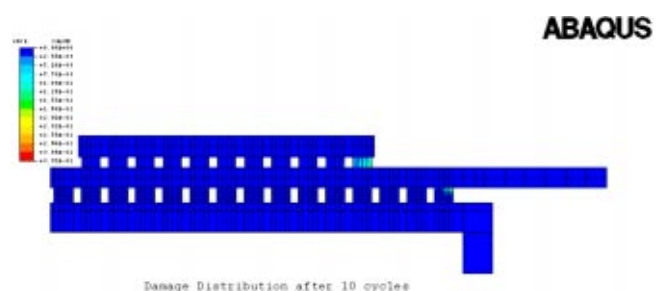


Fig. 19 Damage distribution after 10 thermal cycles (with damage model implemented into ABAQUS)

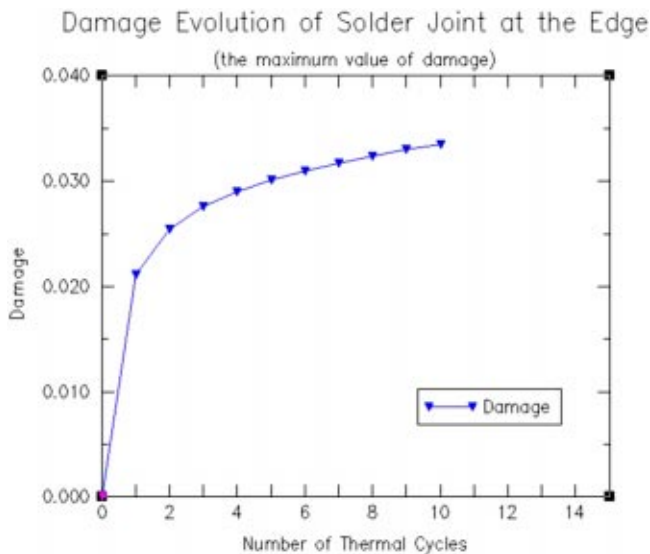


Fig. 20 The evolution of maximum damage under 10 thermal cycles (with damage model implemented into ABAQUS)

criteria by traditional theories. Based on the damage evolution, the accurate fatigue life prediction can be made and the material degradation progress can be monitored by means of computational simulation. However, due to slow data transfer between user defined subroutine and ABAQUS each thermal cycle takes 18.1 h on a 100-MHz Sun Sparc Station.

4 Conclusions

A computational tool with damage-coupled viscoplastic constitutive model has been proposed and implemented into ABAQUS through user defined material subroutine. Using computational simulations, cost of experimental reliability studies on new generation packages can be reduced significantly. The FEA simulation of thermo-mechanical response of Pb37/Sn63 solder joints in BGA electronic package under thermal cyclic loading was compared with the test data. A comparison of FEA results with Moiré interferometry measurements show good correlations. The objective of the implementation is to provide a computational tool for fatigue life predictions of real-life solder joints in electronic package. This work can facilitate numerical simulation of the progressive degradation of eutectic solder interconnections in electronic package under thermo-mechanical fatigue loading without need for extensive testing.

Acknowledgments

This research project is partially sponsored by a grant from the National Science Foundation GOALI program, CMS-9908016 and by the Office of Naval Research Advanced Electrical Power Systems program.

References

[1] Zhao, Y., Basaran, C., Cartwright, A., and Dishongh, T., 1999, "Thermomechanical Behavior of Micron Scale Solder Joints: an Experiment Observation," *J. Mech. Behav. Mater.*, **10**, pp. 135–146.
 [2] Busso, E. P., Kitano, M., and Kamazawa, M., 1992, "A Visco-Plastic Constitutive Model for 60/40 Tin-Lead Solder Used in IC Package Joints," *ASME J. Eng. Mater. Technol.*, **114**, pp. 331–337.
 [3] Dasgupta, A., Oyan, C., Barker, D., and Pecht, M., 1992, "Solder Creep-

Fatigue Analysis by an Energy-Partitioning Approach," *ASME J. Electron. Packag.*, **114**, pp. 152–160.
 [4] Frear, D., Morgan, H., Burchett, S., and Lau, J., 1994, *The Mechanics of Solder Alloy Interconnects*. Chapman & Hall, New York, NY.
 [5] McDowell, D. L., Miller, M. P., and Brooks, D. C., 1994, "A Unified Creep-plasticity Theory for Solder Alloys," *Fatigue Testing of Electronic Materials, ASTM Spec. Tech. Publ.*, **1153**, pp. 42–59.
 [6] Basaran, C., Desai, C. S., and Kundu, T., 1998, "Thermomechanical finite element analysis of problems in electronic packaging using the disturbed state concept. Part I: Theory and formulation," *ASME J. Electron. Packag.*, **120**(1), pp. 41–47.
 [7] Basaran, C., Desai, C. S., and Kundu, T., 1998, "Thermomechanical finite element analysis of problems in electronic packaging using the disturbed state concept. Part II: Verification and Application," *ASME J. Electron. Packag.*, **120**(1), pp. 48–54.
 [8] Chow, C. L., and Yang, F., 1998, "Damage Mechanics Characterization on Fatigue Behavior of a Solder Joint Material," *Proc., ASME International Mechanical Engineering Congress & Exposition*, Anaheim, CA, pp. 1–13
 [9] Basaran, C., and Chandaroy, R., 1998, "Mechanics of Pb40/Sn60 Near-eutectic Solder Alloys Subjected to Vibration," *Appl. Math. Model.*, **22**, pp. 601–627.
 [10] Qian, Z., Ren, W., and Liu, S., 1999, "A damage Coupling Framework of Unified Viscoplasticity for the Fatigue of Solder Alloys," *ASME J. Electron. Packag.*, **21**, pp. 162–168.
 [11] Desai, C., and Siriwardane, H. 1994, *Constitutive Laws for Engineering Materials*, Prentice Hall.
 [12] Basaran, C., Yan, C., 1998, "A Thermodynamic Framework for Damage Mechanics of Solder Joints," *ASME J. Electron. Packag.*, **120**, pp. 379–384.
 [13] Stone, D. S., and Rashid, M. M. 1994, "Constitutive Models," Chap. 4, *The Mechanics of Solder Alloys*, Interconnect, Chapman-Hall.
 [14] Kashyap, P. and Murty, G. S., 1981, "Experimental Constitutive Relations for the High Temperature Deformation of a Pb-Sn Eutectic Alloy," *J. Mater. Sci.*, **50**, pp. 205–213.
 [15] Smithells, C. J., 1983, *Metals Reference Book*, Brandes, 6th Edition.
 [16] Friedel, J., 1964, *Dislocations*, Pergamon Press.
 [17] Armstrong, P. J., and Frederick, C. O., 1996, "A Mathematical Representation of the Multiaxial Bauschinger Effect," G.E.G.B. Report RD/B/N731
 [18] Chaboche, J. L., 1989, "Constitutive Equations for Cyclic Plasticity and Viscoplasticity," *Int. J. Plast.*, **5**, pp. 247–302.
 [19] Kachanov, L. M., 1986, *Introduction of Continuum Damage Mechanics*, Nijhoff (Martinus), Dordrecht.
 [20] Robotnov, Y. N., 1969, "Fundamental Problems in Visco-Plasticity," *Recent Advances in Applied Mechanics*, Academic Press, New York, NY.
 [21] Valanis, K. C., 1997, "Some Thoughts on Thermodynamics of Internal Variables," *Arch. Mech.*, **49**(2), pp. 443–445.
 [22] Chaboche, J. L., and Lesne, P. M., 1988, "A Non-Linear Continuous Fatigue Damage Model," *Fatigue Fract. Eng. Mater. Struct.*, **11**, pp. 1–17.
 [23] Murakami, S., 1988, "Mechanical Modeling of Material Damage," *ASME J. Appl. Mech.*, **55**, pp. 280–286.
 [24] Krajcinovic, D., 1989, "Damage Mechanics," *Mech. Mater.*, **8**, pp. 117–197.
 [25] Ju, J. W., 1989, "On Energy-Based Coupled Elastoplastic Damage Theories: Constitutive Modeling and Computational Aspects," *Int. J. Solids Struct.*, **25**(7), pp. 803–833.
 [26] Lemaitre, J. 1990, *A Course on Damage Mechanics*, Springer LS-DYNA, 1998. LS-DYNA version 940.2 KBS2, Inc.
 [27] Bazant, Z. P., 1991, "Why Continuum Damage is Nonlocal: Micromechanics Arguments," *J. Eng. Mech. Div.*, **117**(5), pp. 1070–1087.
 [28] Chow, C. L., and Chen, X. F., 1992, "An Anisotropic Model of Damage Mechanics Based on Endochronic Theory of Plasticity," *Int. J. Fract.*, **55**, pp. 115–130.
 [29] Voyiadjis, G. Z., and Thisgarajan, G., 1996, "A Damage Cyclic Model for Metal Matrix Composites," *Damage and Interface Debonding in Composites*, Voyiadjis and Allen, eds., Elsevier, New York, NY.
 [30] Solomon, H. D., and Tolksdorf, E. D., 1996, "Energy Approach to the Fatigue of 60/40 Solder: Part II-Influence of Hold Time and Asymmetric Loading," *ASME J. Electron. Packag.*, **188**, pp. 67–71.
 [31] Adams, P. J., 1986, "Thermal Fatigue of Solder Joints in Micro-Electronic Devices," M.S. thesis, Department of Mechanical Engineering, MIT, Cambridge, MA.
 [32] Skipor, A. F., Harren, S. V., and Botsis, J., 1996, "On the Constitutive Response of 63/37 Sn/Pb Eutectic Solder," *ASME J. Eng. Mater. Technol.*, **118**, pp. 1–11.
 [33] Solomon, H. D., 1989, "Strain-Life Behavior in 60/40 Solder," *ASME J. Electron. Packag.*, **111**, pp. 75–82.
 [34] Basaran, C., and Zhao, Y., "Mesh Sensitivity and FEA for Multilayered Electronic Packaging" *ASME J. Electron. Packag.*, **123**, No. (3), pp. 218–224.
 [35] Zhao, Y., Basaran, C., Cartwright, A., and Dishongh, T., 2000, "Thermomechanical Behavior of Micron Scale Solder Joints under Dynamic Loads," *Mech. Mater.*, **32**(3), pp. 161–173.